Lab on a Chip

Accepted Manuscript

ROYAL SOCIETY OF CHEMISTRY

www.rsc.org/loc

Lab on a Chip

RSCPublishing

PAPER

MICROFLUIDIC BEAD-BASED DIODES WITH TARGETED CIRCULAR MICROCHANNELS FOR LOW REYNOLDS NUMBER APPLICATIONS

Cite this: DOI: 10.1039/x0xx00000x

Received 00th January 2012,
Accepted 00th January 2012

DOI: 10.1039/x0xx00000x

www.rsc.org/

Ryan D. Sochol*[a], Albert Lu[b], Jonathan Lei[a], Kosuke Iwai[a], Luke P. Lee[b] and Liwei Lin[a]

Self-regulating fluidic components are critical to the advancement of microfluidic processors for chemical and biological applications, such as sample preparation on chip, point-of-care molecular diagnostics, and implantable drug delivery devices. Although researchers have developed a wide range of components to enable flow rectification in fluidic systems, engineering microfluidic diodes that function at the low *Reynolds number* (*Re*) flows and smaller scales of emerging micro/nanofluidic platforms has remained a considerable challenge. Recently, researchers have demonstrated microfluidic diodes that utilize high numbers of suspended microbeads as dynamic resistive elements; however, using spherical particles to block fluid flow through rectangular microchannels is inherently limited. To overcome this issue, here we present a single-layer microfluidic bead-based diode (18 μm in height) that uses a targeted circular-shaped microchannel for the docking of a single microbead (15 μm in diameter) to rectify fluid flow under low *Re* conditions. Three-dimensional simulations and experimental results revealed that adjusting the docking channel geometry and size to better match the suspended microbead greatly increased the *Diodicity* (*Di*) performance. Arraying multiple bead-based diodes in parallel was found to adversely affect system efficacy, while arraying multiple diodes in series was observed to enhance device performance. In particular, systems consisting of four microfluidic bead-based diodes with targeted circular-shaped docking channels in series revealed average *Di's* ranging from 2.72±0.41 to 10.21±1.53 corresponding to *Re* varying from 0.1 to 0.6.

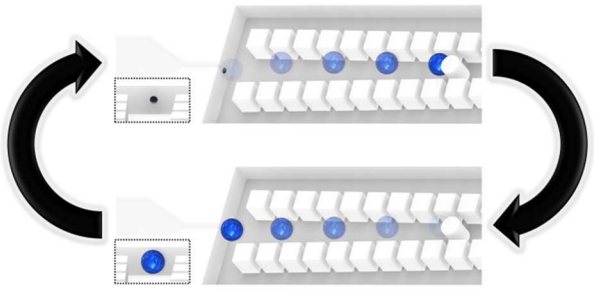

Table of Contents Entry A microfluidic bead-based diode that uses a targeted circular-shaped microchannel for docking a suspended microbead is presented for rectifying fluid flow under low *Reynolds number* conditions.

Lab on a Chip

RSCPublishing

PAPER

Cite this: DOI: 10.1039/x0xx00000x

Received 00th January 2012,
Accepted 00th January 2012

DOI: 10.1039/x0xx00000x

www.rsc.org/

MICROFLUIDIC BEAD-BASED DIODES WITH TARGETED CIRCULAR MICROCHANNELS FOR LOW REYNOLDS NUMBER APPLICATIONS

Ryan D. Sochol*[,a], Albert Lu[b], Jonathan Lei[a], Kosuke Iwai[a], Luke P. Lee[b] and Liwei Lin[a]

Self-regulating fluidic components are critical to the advancement of microfluidic processors for chemical and biological applications, such as sample preparation on chip, point-of-care molecular diagnostics, and implantable drug delivery devices. Although researchers have developed a wide range of components to enable flow rectification in fluidic systems, engineering microfluidic diodes that function at the low *Reynolds number* (*Re*) flows and smaller scales of emerging micro/nanofluidic platforms has remained a considerable challenge. Recently, researchers have demonstrated microfluidic diodes that utilize high numbers of suspended microbeads as dynamic resistive elements; however, using spherical particles to block fluid flow through rectangular microchannels is inherently limited. To overcome this issue, here we present a single-layer microfluidic bead-based diode (18 μm in height) that uses a targeted circular-shaped microchannel for the docking of a single microbead (15 μm in diameter) to rectify fluid flow under low *Re* conditions. Three-dimensional simulations and experimental results revealed that adjusting the docking channel geometry and size to better match the suspended microbead greatly increased the *Diodicity* (*Di*) performance. Arraying multiple bead-based diodes in parallel was found to adversely affect system efficacy, while arraying multiple diodes in series was observed to enhance device performance. In particular, systems consisting of four microfluidic bead-based diodes with targeted circular-shaped docking channels in series revealed average *Di's* ranging from 2.72±0.41 to 10.21±1.53 corresponding to *Re* varying from 0.1 to 0.6.

Introduction

Passive fluid flow rectifiers (*i.e.*, fluidic diodes) are vital to a variety of chemical and biological systems, such as mammalian hearts and veins, micropumps, and integrated fluidic circuits[1-4]. Although micro and nanoscale fluidic systems offer significant benefits for biochemical applications (*e.g.*, low reagent volumes, rapid reaction kinetics, and high control of environmental conditions)[5-8], difficulties associated with flow rectification at such scales have hindered progress in this field[9-11]. For example, microscale "fixed-geometry" valves, such as diffusers and Tesla valves, exploit fluidic inertia to achieve *Di's* (*i.e.*, the ratio of forward flow *versus* reverse flow[9]) of up to 4.5 for *Re* ranging from 10 to 200[11, 12]; however, at lower *Re*, the contribution of the non-linear inertial term of the Navier-Stokes equations becomes negligible, thereby rendering such valves ineffective[10-13]. Specifically, for $Re < 10$ fluid flow, fixed-geometry valves exhibit *Di's* approaching 1, which results in functionality that is closer to that of a fluidic resistor than a diode[11, 12]. Consequently, recent research has focused on employing soft lithography-based microfabrication techniques to create passive diodic components that utilize dynamic resistive elements[14-16]. In particular, a number of researchers have engineered cantilever-type "flap" valves, which include an anchored elastomeric flap that deforms (based on the magnitude of inputted fluid flow) to either: (*i*) deflect away from an orifice to promote forward flow, or (*ii*) close against the orifice to limit reverse flow[14-17]. For *Re* ranging from roughly 1 to 35, researchers have reported *Di's* up to 4.6; however, because fluidic forces are needed to deform the flaps, prior works have found that such valves fail at lower *Re* (*e.g.*, $Re < 0.3$)[10, 14]. Additionally, valves that utilize elastomeric resistive components are primarily manufactured *via* multi-layer micro-fabrication processes[14-17], which suffer from increased costs, time, and labor compared to single-layer lithographic processes.

To bypass the aforementioned limitations associated with fluidic diodes that utilize deformable resistive elements (*e.g.*, flaps and membranes), researchers have also focused on adapting "ball" valves for microfluidic applications[18-22]. In particular, prior reports have demonstrated micropumps that use two ball valves in series to generate fluid flow in a single direction[18-21]. In such systems, singular millimeter-scale balls (*e.g.*, 0.4-1.2 mm in diameter) were used in each of the ball valves, primarily through manual insertion. Additionally, a wide range of fabrication techniques were employed to construct the valves, such as combining tapered plastic micropipettes with heat-shrink tubing[18], adapting multi-layer photolithography and soft lithography methods[19, 20], and using stereolithography processes[21]. Despite significant progress however, such systems remain limited for biomedical applications (*e.g.*, ocular drug delivery implants) that require fluidic diodes that are: (*i*) structurally thin (*e.g.*, < 100 μm), and (*ii*) function at low pressures and/or *Re*[22]. To enable functionality in accordance with these design criteria, Ou *et al.* recently introduced a single-layer microfluidic bead-based diode with rectangular microchannels that utilized up to 850 suspended microbeads (20 μm in diameter) to achieve *Di's* of up to 18 under *Re* < 1 conditions[22]. One challenge associated with implementing this technique is that consistently loading similar numbers of microbeads into the system (*e.g.*, *via* manual observation) can be difficult and labour-intensive; however, a more critical issue is that using spherical microparticles to block fluid flow through rectangular microchannels is inherently flawed[22, 23]. Thus, here we present a single-layer microfluidic bead-based diode that includes a single suspended polystyrene microbead (15 μm in diameter) and a targeted circular-shaped microchannel for microbead docking. Previously, we observed that altering the docking channel geometry to better mimic the spherical microbead shape offered one mode through which device performance could be improved; however, other potential enhancement modes, such as serial or parallel arraying of microfluidic bead-based diode components, were not investigated[24, 25]. Additionally, the theoretical relationship between the microbead docking channel geometry and the corresponding *Di* performance was not examined[25]. Thus, in this work, both theoretical simulations and experimental approaches were employed to investigate: (*i*) the resistive contribution of a single suspended microbead *versus* varying docking channel geometries, (*ii*) the potential enhancement in *Di* performance associated with shifting from a docking channel with a rectangular cross-section to a circular-shaped cross-section, and (*iii*) the effects of arraying multiple systems in parallel and in series. Device architectures with one, two, and four microfluidic bead-based diodes in parallel and in series (for both rectangular-shaped and targeted circular-shaped docking channels) were constructed and characterized. The theoretical and experimental results provide a necessary foundation for future microfluidic bead-based diodes, which offer a powerful methodology to achieve flow rectification in emerging lab-on-a-chip technologies.

Materials and methods

Microfluidic Bead-Based Diode Concepts

The operating principle of the microfluidic bead-based diode in this work is similar to that of a macroscale ball check valve. For the forward flow case, the single suspended microbead releases from the entrance of the docking channel to promote fluid flow through the system (Fig. 1a). After release, the microbead is retained within the diode chamber due to the surrounding microposts, which act as a physical barrier. A circular micropost is included to prevent the suspended microbead from being lodged between the two sets of arrayed square-shaped microposts (separation angle = 2°). For cases in which the flow polarity is reversed, the microbead is transported to the entrance of the docking channel, which increases the fluidic resistance, thereby reducing the flow of fluid through the diode (Fig. 1b). This process occurs passively and is based exclusively on changes in the fluid flow polarity.

Although the majority of the single-layer device consists of rectangular microchannels, the diode chamber includes a circular-shaped channel for microbead docking. To achieve this targeted circular-shaped docking channel, we adapted a methodology originally introduced by Abdelgawad *et al.*[26]. Initially, uncured poly(dimethylsiloxane) (PDMS) is loaded into a rectangular docking channel (Fig. 2a, b). Once the uncured PDMS fills the docking channel completely,

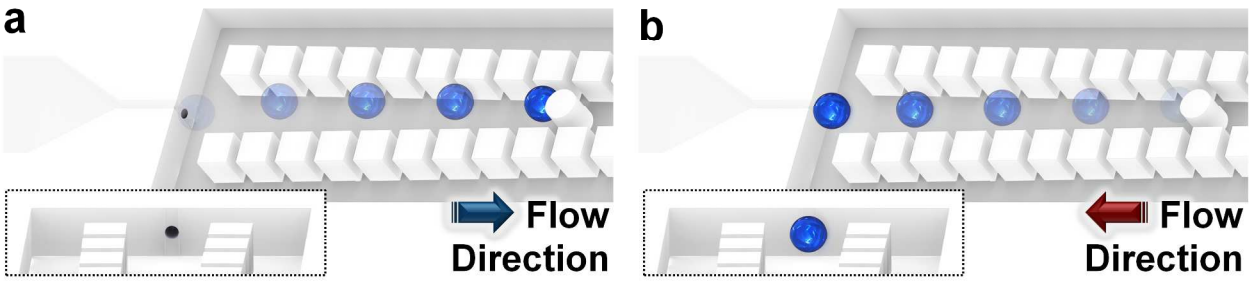

Figure 1. Conceptual illustrations of the microfluidic bead-based diode with a targeted circular-shaped docking channel. (a) During forward flow, the single suspended microbead is released from the entrance of the docking position to enable fluid flow through the microchannel. The microbead remains within the diode chamber. (b) During reverse flow, the microbead is immobilized in the docking site, thereby obstructing fluid flow through the microchannel. This process functions autonomously based on the fluid flow polarity. Insets show expanded views of the circular-shaped docking channel.

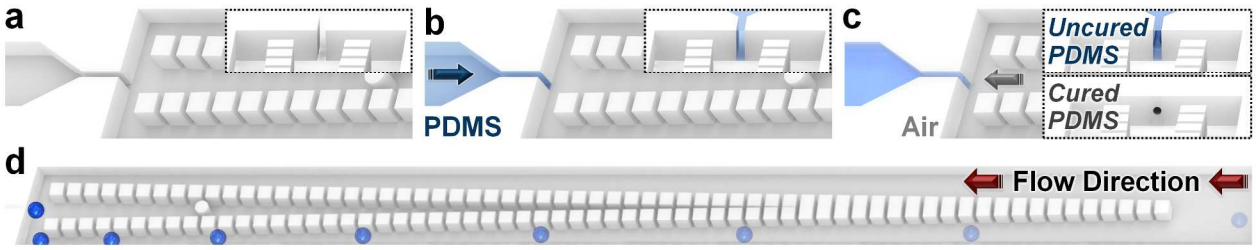

Figure 2. Conceptual illustrations for (a-c) selectively fabricating a circular-shaped docking channel and (d) pre-loading a single suspended microbead. (a) Initially, the microsystem includes rectangular-shaped microchannel cross-sections. (b) A separate inlet is used to load uncured (*i.e.*, liquid-phase) poly(dimethylsiloxane) (PDMS; *blue*) into the docking channel. (c) After the PDMS has reached the base of the docking channel, pressurized air is inputted (*via* the opposite direction) to displace the uncured PDMS (*blue*; *top inset*), leaving behind a circular-shaped cross-section after curing (*grey*; *bottom inset*). (a-c) Insets show expanded views of the microbead docking channel; The illustrated change in colour of PDMS is for conceptual purposes only. (d) Under reverse flow, a single suspended polystyrene microbead is pre-loaded into the diode chamber. The micropost array railing (μPAR) technique[27] prevents the microbead from being immobilized prior to reaching the entrance of the docking channel.

pressurized air is inputted from the opposite direction during the curing process in order to displace a fraction of the PDMS, while leaving behind a circular-shaped cross-section (Fig. 2c).

One of the challenges associated with microfluidic bead-based diodes is ensuring that the loaded microbead remains within the system. At larger scales, other techniques require manual placement of the dynamic spherical resistive element[18-20]; however, such methods are not practical at the smaller scales (*e.g.*, < 25 μm). Previously, we presented a micropost array railing (μPAR) technique for passively transporting suspended microparticles (*e.g.*, microbeads and endothelial cells) between discrete, adjacent flow streams[27]. In this work, we exploit a characteristic of the μPAR technique – the ability to displace a microbead from its original flow stream – to achieve a "one-way track" for pre-loading a single suspended microbead into the diode chamber. Under reverse flow, the suspended microbead is passively guided along the micropost array rails (*i.e.*, without being immobilized) until it is transported to the entrance of the docking channel within the diode chamber (Fig. 2d). Thereafter, the microbead remains within the chamber regardless of the flow polarity (Fig. 1).

Microfabrication

The overall microdevices were fabricated *via* a standard, single-layer soft lithography process as described previously[27]. The negative photoresist, SU-8 2010 (MicroChem, Newton, MA), was spin-coated onto standard 4" Silicon wafers. Microfeatures were defined *via* contact photolithography (Hybralign, Series 400, Optical Associates, Milpitas, CA). Using the developed photoresist as a negative master, the device was micromolded with the silicone elastomer, PDMS, at a 10:1 (base : curing agent) ratio (Sylgard 184, Dow Corning, Corning, NY). After curing at 55 °C for at least two hours, the PDMS was removed from the negative master and individual devices were cut from the PDMS. Ports for the catheter couplers (#SP20/12, Instech Laboratories, Plymouth Meeting, PA) were punched at all four input locations, corresponding to the: (*i*) PDMS loading inlet, (*ii*) microbead loading inlet, (*iii*) forward flow fluid inlet, and (*iv*) reverse flow fluid inlet. The PDMS devices were cleaned and covalently bonded to Fisherbrand glass microscope slides (Fisher Scientific, Pittsburgh, PA) *via* UV ozone treatment (UVO cleaner, model 42, Jetlight Company, Irvine, CA).

The devices were designed for 15.2 μm diameter polystyrene microbeads (#SVP-150-4, Spherotech, Inc., Lake Forest, IL). Due to the polydispersity of the microbeads (corresponding to a standard deviation of ±2.2 μm), the heights of the microchannels were set at 18 μm. A filter was integrated into the inlets to limit large microparticles (> 16 μm in diameter) and debris from entering the channels. The docking channel was 5 μm in width. The arrayed microposts in the diode chamber were 15×15 μm^2, and the gaps between microposts were 5 μm. The microposts were arrayed at ±1° with respect to the flow direction to ensure effective railing because larger angles have previously been demonstrated to induce microbead immobilization in the gaps between arrayed microposts[27]. The single circular-shaped micropost was 15 μm in diameter. SEM micrographs of a fabricated microfluidic bead-based diode with a rectangular docking channel are shown in ESI Fig. 1. Previously, we experimentally tested singular diode systems; however, additional system designs, such as those with multiple diodes arrayed either in parallel or in series, were not examined[24, 25]. To study the potential effects of such configurations, in this work, ten different system architectures were fabricated for testing, corresponding to microdevices with one, two, and four microfluidic bead-based diodes in parallel and in series, for both rectangular and targeted circular-shaped microbead docking channels.

Targeted circular-shaped microbead docking channel

The microfluidic device was designed with a separate inlet (on the reverse flow fluid inlet side of the diode) for loading of the uncured PDMS (10:1 base : curing agent ratio; Dow Corning). The microfluidic device was placed in a vacuum for at least 5 min while all of the inlet/outlet ports were sealed with Scotch tape, except for the PDMS loading inlet. After removing the device from the vacuum, uncured PDMS was vacuum-loaded

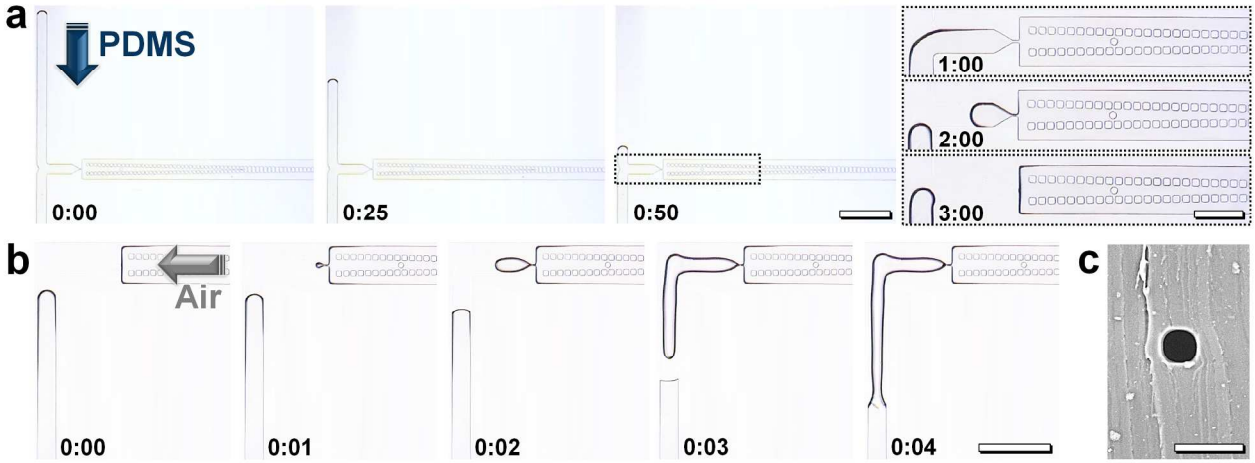

Figure 3. Experimental results for selectively fabricating a circular-shaped docking microchannel. (a) Uncured PDMS is vacuum loaded into the docking channel during optical monitoring over the course of three minutes. Expanded views show the diode chamber. (b) After the PDMS has reached the base of the docking channel, pressurized air is inputted into the device during thermal curing of the PDMS. Units = seconds. (c) SEM micrograph of the cross-section of a fabricated docking channel. Scale Bars = (a) 250 μm, (*Inset*) 100 μm, (b) 200 μm, (c) 10 μm. ESI Movie 1 shows video of this process.

via the PDMS loading inlet. Fig. 3a shows experimental results for the PDMS vacuum-loading process, which was accomplished within approximately 5 min and monitored visually. Once the PDMS was observed to reach the base of the diode docking channel, the tape was removed from the forward flow fluid inlet and pressurized air (approximately 100 kPa) was inputted from that inlet, while a catheter plug (#SP20/12, Instech) was inserted into the PDMS loading port and the tape from the reverse flow fluid inlet was removed. The device was then placed on a hot plate (set at 150 °C) for up to 30 min to cure the PDMS, which consequently sealed the PDMS loading inlet. Fig. 3b shows sequential micrographs of the PDMS-displacement process. ESI Movie 1 includes video of this process for a system with one diode. Fig. 3c shows an SEM micrograph of the cross-section of a fabricated microbead docking channel. For systems with multiple diodes arrayed in series, the targeted circular-shaped docking channel fabrication process was executed independently and separately (*i.e.*, one-at-a-time). In contrast, the multiple circular-shaped docking microchannels of systems with two and four diodes arrayed in parallel could be fabricated simultaneously (ESI Fig. 2). One consequence of the PDMS-displacement process is that a small amount of PDMS enters the main channel (Fig. 3b – *bottom-left channel*), resulting in a rectangular-to-circular microchannel cross-section transition zone. Although such phenomena would slightly increase the resistance through the system, flow rectification behaviour would not be affected.

Microbead loading

A separate microbead loading inlet was used to pre-load a single suspended polystyrene microbead into the diode chamber from the reverse flow direction. A diluted microbead suspension (approximately 1 bead/μL) was inputted at a flow rate of 1 μL/min. The pre-loading process was monitored visually to ensure that only a single microbead entered the diode chamber. As shown in ESI Fig. 3 and ESI Movie 2, the μPAR technique prevented inputted microbeads from immobilizing prior to reaching the entrance of the docking channel of the diode chamber. After the microbead was immobilized in the docking position, DI water was inputted from the forward flow inlet while the microbead loading inlet was sealed with a catheter plug. As a result, the only remaining accessible ports were the forward flow and reverse flow inlets. Similar to the protocol for the circular-shaped docking channel fabrication process, microbeads were pre-loaded independently into systems with multiple diodes in series; however, for systems with multiple diodes in parallel, the microbeads were loaded simultaneously. For example, ESI Fig. 4 shows sequential micrographs of four microbeads being loaded into a system consisting of four diodes with circular-shaped channels in parallel. ESI Fig. 5 includes fabrication results following the microbead pre-loading process for systems with two and four microfluidic diodes in series and in parallel.

Theoretical simulations

Three-dimensional pressure field simulations were generated using the commercial finite element analysis software, COMSOL Multiphysics version 4.2. Previously, the theoretical relationship between the geometry of the microbead docking channel and microfluidic bead-based diode performance was not examined[24, 25]. To investigate the effects of docking channel geometry on flow rectification performance, here, microfluidic bead-based diodes with five distinct docking channel geometries were modelled: (*i*) an 18 × 5 μm^2 rectangular cross-section, (*ii*) a 15.5 × 5 μm^2 obround-shaped cross-section, (*iii*) a 13 × 5 μm^2 obround-shaped cross-section, (*iv*) a 10.5 × 5 μm^2 obround-shaped cross-section, and (*v*) an 8 × 5 μm^2 obround-shaped cross-section (ESI Fig. 6). A spherical docking channel cross-section (5 μm in diameter) was not modelled because such a geometry would result in a

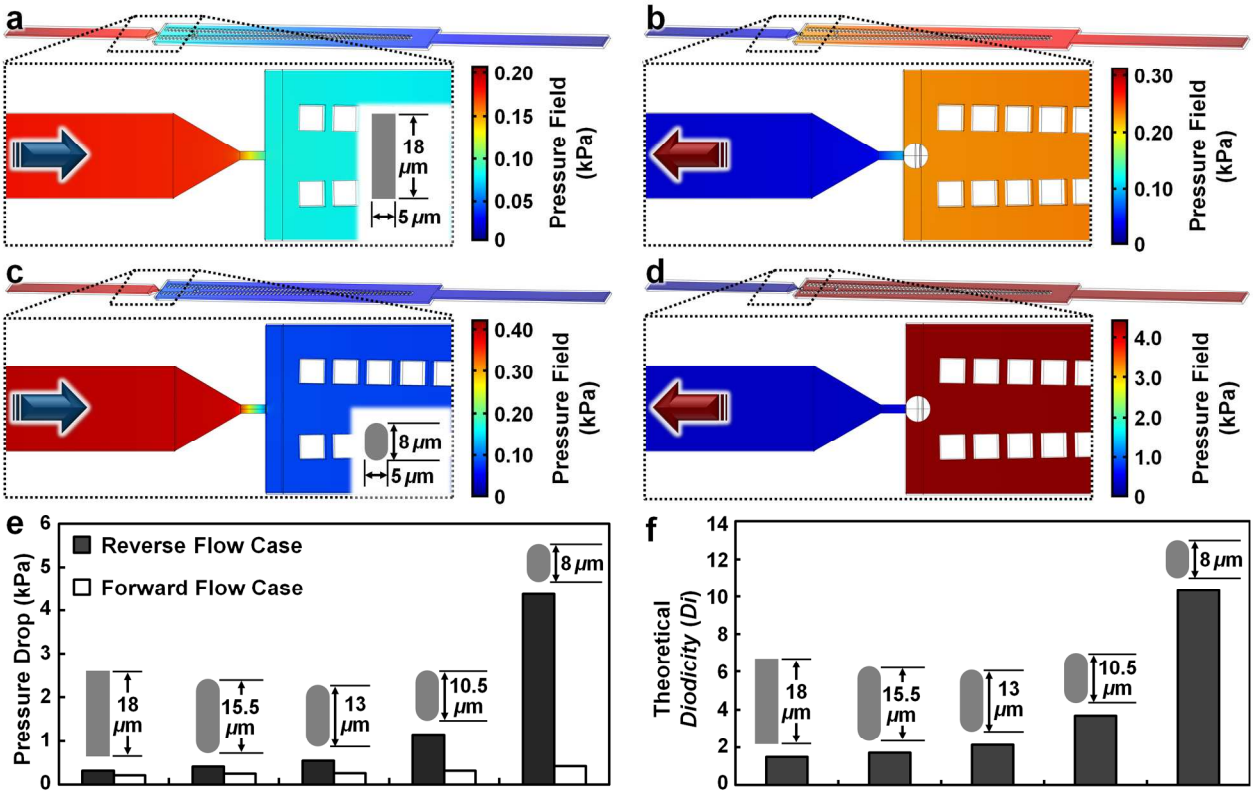

Figure 4. Theoretical results for three-dimensional COMSOL Multiphysics simulations of microfluidic bead-based diodes with varying microbead docking channel geometries. (a, b) Pressure field simulation results for a system with an 18×5 μm^2 rectangular docking channel cross-section (*inset*) corresponding to the (a) forward flow and (b) reverse flow cases. (c, d) Pressure field simulation results for a system with an 8×5 μm^2 obround-shaped docking channel cross-section (*inset*) corresponding to the (c) forward flow and (d) reverse flow cases. (e) Theoretical pressure drop *versus* varying docking channel geometries (5 μm in width). (f) Theoretical *Diodicity* (*Di*) *versus* varying docking channel geometries (5 μm in width). ESI Figure 7 includes simulation results corresponding to additional docking channel geometries.

pressure drop of infinity for the reverse flow case. An ideal microsphere (15 μm in diameter) was placed at half the height of the microchannel (18 μm in height) at the entrance of the docking channel for the reverse flow simulations, and in contact with the circular micropost (away from the entrance of the docking channel) for the forward flow simulations. The three-dimensional "Incompressible Navier–Stokes" application mode for steady-state analysis was used for all simulations. Water ($\rho = 10^3$ kg/m^3; $\eta = 10^{-3}$ Pa•s) was modelled in all of the fluidic simulations. The output pressure was set at 0 Pa, while all other boundary conditions were set to have no-slip conditions. The mesh sizes were refined to ensure that the simulation results were independent of mesh size. All of the simulations included mesh sizes of 8.07±2.73×10^6 tetrahedral elements (ESI Fig. 6). The input fluid velocity was initially varied to examine the potential for flow rectification disparities over a range of $0.025 \leq Re \leq 25$; however, the diodic behaviour of the simulations was found to be consistent despite changes in the flow magnitude within this range. For the simulations presented in this work, the input fluid velocities were set at 5 mm/s (corresponding to a *Re* of approximately 0.25).

Experimental setup and analysis

All experiments were conducted under room temperature environment (20-25 °C). To limit the immobilization of microbeads at locations other than the docking channel, the polysorbate surfactant, Tween 20 (10% in PBS, Fisher), was vacuum loaded into the device prior to operation for a 15 min incubation period. To regulate the input pressures while simultaneously monitoring the flow rates of fluid through the microdevices, we used the MAESFLO system, which includes both the Microfluidic Flow Control System (MFCS) and the FLOWELL microfluidic flow sensor (Fluigent, Paris, France). Experiments for the forward flow case (the microbead is not in the docking position) and the reverse flow case (the microbead is in the docking position) were performed for each of the ten system designs (*i.e.*, one, two, and four diodes in parallel and in series, for both rectangular and circular-shaped microbead docking channels). The pressures and flow rates from the experiments were used to quantify the *Di* at varying *Re* as:

$$Di_{Re} = \frac{\Delta P_{Reverse,Re}}{\Delta P_{Forward,Re}} \quad (1)$$

where $\Delta P_{Reverse,Re}$ and $\Delta P_{Forward,Re}$ denote the pressure drops across the microfluidic bead-based diode corresponding to the same *Re* conditions for the reverse flow and forward flow

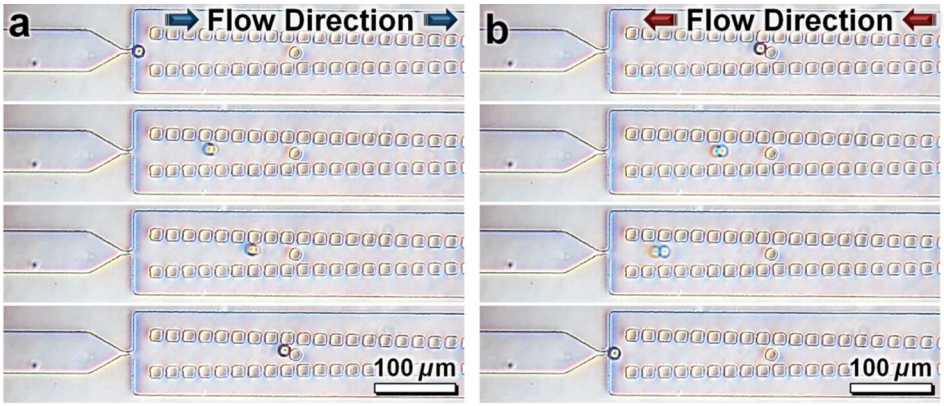

Figure 5. Sequential phase-contrast micrographs of experimental results for microbead dynamics during the operation of the microfluidic bead-based diode. (a) During forward flow, the suspended microbead releases from the entrance of the docking channel, but remains within the diode chamber due to the micropost array rails. (b) During reverse flow, the suspended microbead is transported to the entrance of the docking channel. ESI Movie 3 shows real-time video of this process.

cases, respectively. Quantified experimental results are presented in the text as mean ± s.e.m. All micrographs and movies were captured with a fluorescent inverted microscope (Motic AE31, Motic Instruments, Inc., Richmond, BC, Canada) connected to a Micropublisher 5.0 RTV charge-coupled device (CCD) camera (QImaging, Burnaby, BC, Canada) and calibrated with QCapturePro (QImaging).

Results and discussion

Theoretical Simulations

Three-dimensional COMSOL Multiphysics fluid dynamics simulations were performed for several microfluidic bead-based diode designs to investigate the effects of docking channel geometry and size on device performance. For the system with an 18×5 μm^2 rectangular microchannel, the simulation results revealed a slight difference between the pressure drops for the forward flow (Fig. 4a) and reverse flow (Fig. 4b) cases. Decreasing the size of the docking channel was found to increase this difference to some extent (ESI Fig. 7); however, decreasing the height to achieve an 8×5 μm^2 obround-shaped cross-section resulted in an increase in the difference between the forward flow (Fig. 4c) and reverse flow (Fig. 4d) pressure drops by an order of magnitude. The theoretical pressure drops corresponding to each of the docking channel geometries modelled are shown in Fig. 4e. Although the forward flow pressure drop was found to increase by a factor of 2 (at maximum) for the simulations performed, the reverse flow pressure drop for the 8×5 μm^2 obround-shaped docking channel was 14 times larger than the 18×5 μm^2 rectangular docking channel (Fig. 4e). This resulted in an increase in the theoretical *Di* performance from approximately 1.50 for the 18×5 μm^2 rectangular docking channel to 10.33 for the 8×5 μm^2 obround-shaped docking channel (Fig. 4f). These results suggest that reducing the size of the docking channel (approaching a 5 μm-in-diameter circular cross-section) offers a powerful geometric mode though which the *Di* performance can be enhanced.

Microfluidic bead-based diode functionality and characterization

One of the critical requirements of the microfluidic bead-based diode in this work is the ability to retain the single suspended microbead within the diode chamber following the pre-loading process. To examine this capability, the flow polarity was repeatedly cycled between forward and reverse flows while visually monitoring the location of the microbead. Sequential micrographs and real-time video of microbead dynamics within the microfluidic bead-based diode are shown in Figure 5 and ESI Movie 3, respectively. Under forward flow conditions, the microbead was not found to follow the original flow path observed during the pre-loading process (ESI Fig. 3; ESI Movie 2). Rather, the released microbead consistently remained within the diode chamber, temporarily immobilizing between the circular micropost and the arrayed square-shaped microposts (with no observed preference in the top or bottom position) (Fig. 5a). The forward flow path of the microbead was found to differ from the reverse flow case. Specifically, under reverse flow, the microbead followed a linear path toward the entrance of the docking channel and subsequently immobilized (Fig. 5b). For forward flow however, the microbead was typically transported to the micropost array rails first, and then guided along the rails until its motion was physically inhibited by the circular micropost (Fig. 5a). The displacement of the microbead both to and from the docking channel (depending on the flow polarity) was found to initiate at flow rates corresponding to $Re = 0.1$ (*i.e.*, the lowest flow achievable for the experimental setup) and occurred over a timespan within five seconds at maximum (ESI Movie 3). Despite the asymmetric nature of the polarity-based flow path, device functionality was not impacted as the microbead was effectively retained within the diode chamber through repeated external switches of the flow polarity (ESI Movie 3).

To experimentally investigate the polarity-based difference in flow behavior for the microfluidic bead-based diode, the input pressure was gradually increased by 0.1 kPa from approximately 0.2 kPa up to 5 kPa for both the forward and reverse flow directions while monitoring the resulting magnitude of fluid flow. Five distinct microfluidic bead-based diode configurations were experimentally tested for both the rectangular and targeted circular-shaped docking channel cases (for a total of ten different system designs).

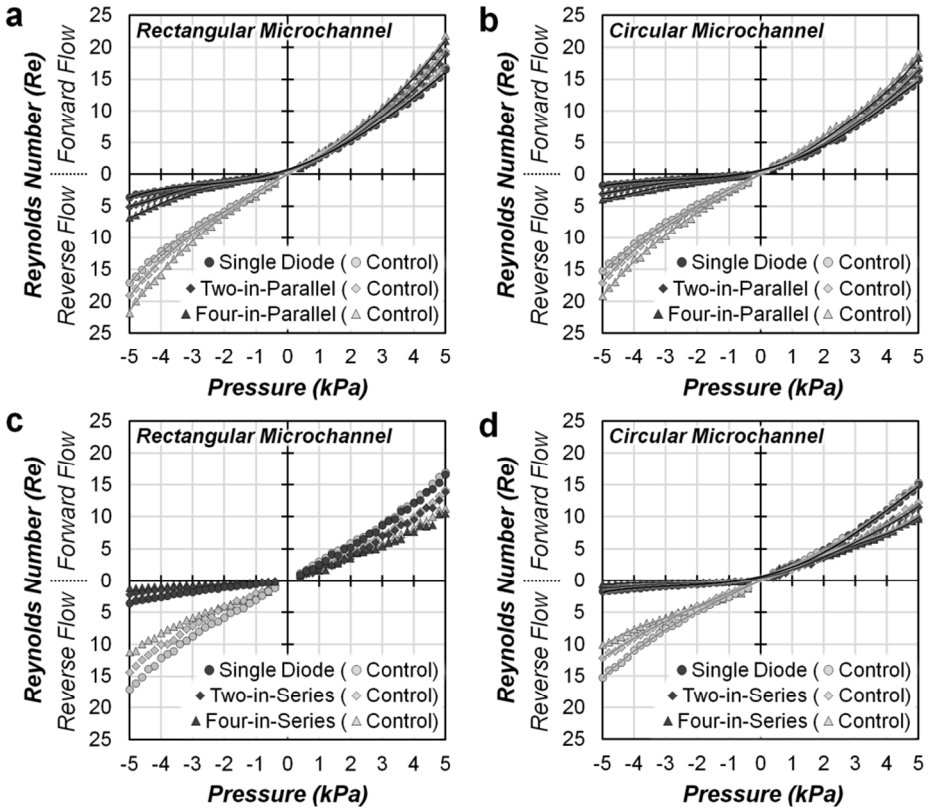

Figure 6. Experimental results for *Reynolds number* (*Re*) flow *versus* pressure for system architectures with one, two, and four microfluidic bead-based diodes (a, b) in parallel, and (c, d) in series. (a, c) Systems with rectangular-shaped microbead docking channels; (b, d) Systems with targeted circular-shaped microbead docking channels; Light grey denotes control systems without a loaded microbead; Dark grey denotes systems with a loaded microbead.

Flow measurements for each system were performed up to three times for bead-based experiments as well as negative control experiments, which did not include microbeads within the diode chamber. Fig. 6a and 6b include experimental results for pressure *versus Re* corresponding to systems with one, two, and four devices in parallel for the rectangular and circular-shaped docking channel cases, respectively. For both the forward (positive) and reverse (negative) flow directions, the same pressures resulted in smaller flow rates for systems with targeted circular-shaped docking channels compared to systems with uniform rectangular channels. For positive pressures, control experiments revealed that the removal of the microbeads had little effect on the flow behaviour. For negative pressures however, the addition of the suspended microbeads was found to decrease the magnitude of fluid flow by up to 78.3% for the rectangular case and 88.3% for the circular case. The experimental results also revealed that increasing the number of microfluidic bead-based diodes in parallel appeared to decrease the fluidic resistance to some extent, resulting in comparatively larger flow rates for the same input pressures (Fig. 6a, b). In contrast, larger numbers of microfluidic bead-based diodes in series resulted in slightly lower flow rates for the same input pressures (Fig. 6c, d). Across all of the systems tested, the flow *versus* pressure response was slightly non-linear, with the fluidic resistance appearing to decrease with increasing pressure (Fig. 6). One potential basis for this phenomenon is that the devices were constructed from PDMS, which is a flexible elastomer. Consequently, higher input pressures could cause the PDMS to deform (*i.e.*, increase in height and width), thereby decreasing the overall fluidic resistance of the system, which would promote fluid flow. The trend of suspended microbeads having little effect on the forward flow behaviour was consistent for multiple systems in series; however, the difference between the bead-based diodes and the control experiments for reverse flow rates for multiple systems in series was greater (Fig. 6c, d). For multiple systems in series, the addition of suspended microbeads resulted in a decrease in the magnitude of fluid flow by up to 88.7% for the rectangular case and 94.2% for the circular case. For the pressure range tested, these results suggest that arraying multiple microfluidic bead-based diodes in series is preferable to using a single diode or arraying multiple diodes in parallel for cases in which limiting backflow is a critical parameter.

Experimental *Diodicity (Di)* Performance

Subsequent to the experimental characterization of *Re versus* pressure drop for the ten microfluidic bead-based diode systems tested (Fig. 6), the corresponding *Di* results were quantified *via* Equation 1. The experimental results for *Di* performance are presented in Figure 7. Systems with targeted circular-shaped docking channels were found to exhibit slightly larger *Di's* compared to systems with uniform rectangular channels. This trend appeared more pronounced with increasing *Re*, particularly for systems with multiple bead-based diodes arrayed in series (Fig. 7c, e); however, such differences were relatively small compared to the behaviour predicted from the theoretical simulations (Fig. 5). This result was primarily due

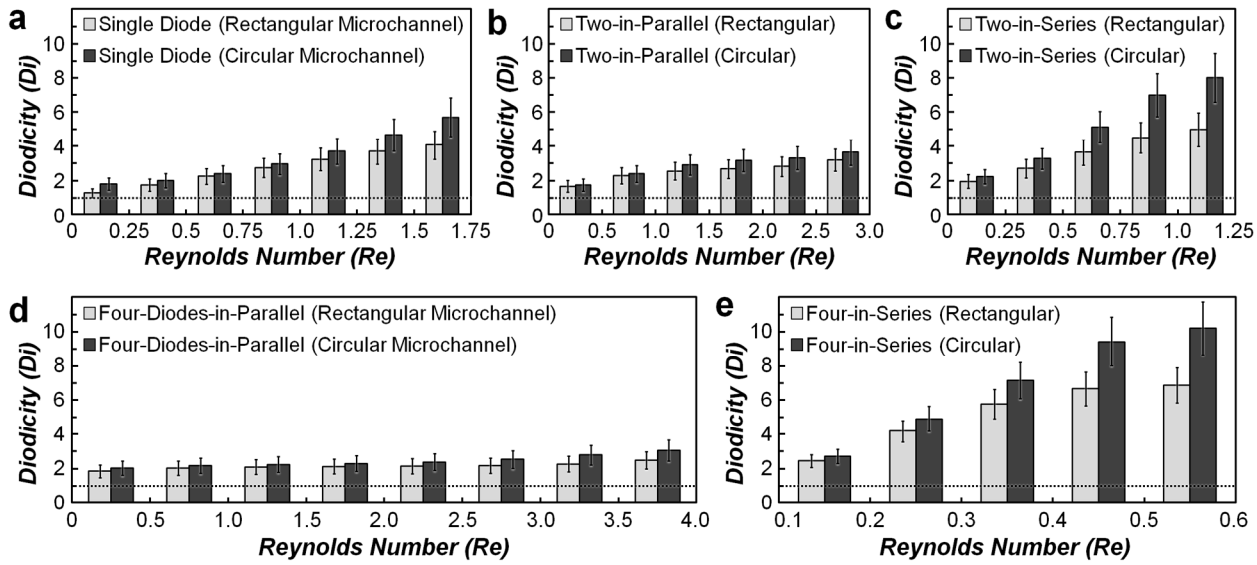

Figure 7. Experimental results for average *Diodicity* (*Di*) performance *versus* varying *Reynolds number* (*Re*) for systems with (a) one, (b, c) two, and (d, e) four microfluidic bead-based diodes (b, d) in parallel and (c, e) in series. Error Bars denote s.e.m.; Light grey denotes systems with rectangular microbead docking channels; Dark grey denotes systems with targeted circular-shaped docking channels; Dotted lines mark $Di = 1$ (*i.e.*, fluidic resistor-like performance); *Di* results were quantified *via* Eq. 1.

to the diodes with rectangular docking channels outperforming the theoretical *Di* of 1.5. For example, systems with uniform rectangular microchannels revealed average experimental *Di's* of up to 4.06±0.81 ($1.5 \leq Re \leq 1.75$), 3.20±0.64 ($2.5 \leq Re \leq 3$), and 2.49±0.50 ($3.5 \leq Re \leq 4$) for systems with one, two, and four microfluidic bead-based diodes in parallel (Fig. 7a, b, d), and up to 4.98±0.99 ($1 \leq Re \leq 1.25$) and 6.88±1.03 ($0.5 \leq Re \leq 0.6$) for systems with two and four diodes in series, respectively (Fig. 7c, e). One potential basis for this result is the aforementioned flexibility of the PDMS. In contrast to the theoretical model, which included a microbead in contact with the edges of a rigid (*i.e.*, non-deformable), rectangular docking channel, the elastomeric PDMS of the fabricated docking channel could have deformed in response to the fluidic forces to enable the suspended microbead to enter farther into the docking channel. Additionally, larger shear stresses impacting a docked microbead could potentially enhance this effect. Under these circumstances, the corresponding fluidic resistance would be increased, which would better limit the flow of fluid during reverse flow. For the forward flow case, deformed PDMS (with increased microchannel dimensions) would decrease the fluidic resistance, thereby promoting the flow of fluid through the system. In combination, these phenomena may have contributed not only to the improved flow rectification performance compared to the simulation results (Fig. 4f), but also to the observed trend of improved *Di* performance with increasing *Re* across all of the systems tested (Fig. 7) – behaviour not observed for the theoretical simulations in which the fluidic resistance remained constant for varying *Re*. Nonetheless, the devices with circular-shaped microbead docking channels yielded the highest *Di's* compared to their rectangular counterparts, which were up to 40%, 23%, and 61% larger for the singular, in parallel, and in series system architectures, respectively (Fig. 7).

The experimental *Di* results revealed two general trends for device configurations with multiple microfluidic bead-based diodes: (*i*) arraying additional systems in parallel appeared to limit the overall *Di* performance (Fig. 7b, d), and (*ii*) arraying additional systems in series appeared to enhance the overall *Di* performance (Fig. 7c, e). For devices with targeted circular-shaped docking channels, the maximum observed average *Di* decreased from 5.70±1.14 ($1.5 \leq Re \leq 1.75$) for a single-device system to 3.64±0.73 ($2.5 \leq Re \leq 3$) and 3.06±0.61 ($3.5 \leq Re \leq 4.0$) for systems with two and four microfluidic bead-based diodes in parallel, respectively (Fig. 7a, b, d). In contrast, the maximum average *Di* was found to increase up to 8.01±1.44 ($1 \leq Re \leq 1.25$) and 10.21±1.53 ($0.5 \leq Re \leq 0.6$) for systems with two and four microfluidic bead-based diodes in series, respectively (Fig. 7c, e). One potential basis for these trends is the effect of microbead polydispersity on resistive performance. Although the theoretical models included uniform microspheres that were placed at exactly half the height of the channel with ideal contact at the docking channel entrance, the microbeads used for experimentation can be polydisperse in both shape and size[23] with the potential for additional variation in the docking behaviour. For cases in which a microbead does not immobilize effectively at the entrance of the docking microchannel, the resistive contribution of the microbead would be reduced, limiting its ability to obstruct reverse fluid flow. Overall, such issues may have contributed to the decreased *Di* performance for the circular-shaped channels during experimentation compared to the theoretical results (Fig. 4f, Fig. 7a). For systems with multiple bead-based diodes in parallel specifically, suboptimal microbead docking would result in reverse flow being directed

to the path of least resistance (through docking microchannels with suboptimal microbead docking), rather than divided equally through each parallel system. As a result, the overall blocking effects of sufficiently docked microbeads would be diminished or negated. Such occurrences could account for the observed decline in *Di* performance associated with larger numbers of bead-based diodes in parallel (Fig. 7b, d). For systems with multiple diodes in series, however, some of these potential bead-based issues could be counteracted by effectively docked microbeads in upstream or downstream systems as reverse flow would always follow the same overall path (*i.e.*, through each docking channel in series), regardless of microbead docking irregularities. Additionally, it is also possible for microbeads to exhibit geometric and/or size-based variations that could contribute to improved device performance, such as through a more complementary microbead-to-docking channel geometry match. Either independently or in combination, such instances offer potential mechanisms underlying the observed enhancement in *Di* performance associated with larger numbers of microfluidic bead-based diodes in series (Fig. 7a, c, e).

Conclusions

Emerging micro/nanofluidic technologies demand robust fluidic components that are capable of functioning effectively not only at smaller scales, but also under the low *Re* flow conditions associated with such sizes. In this work, we presented a microfluidic bead-based diode that utilized a targeted circular-shaped docking channel to improve the geometry match between the dynamic resistive element (*i.e.*, the suspended microbead) and the fluid flow channel. Both theoretical simulations and quantified experimental results demonstrated that adjusting the shape and size of the docking channel to better mimic the geometry of the suspended microbead offer effective means for enhancing device performance (Fig. 4; Fig. 6; Fig. 7). In particular, the simulation results revealed that decreasing the microbead docking channel geometry from an 18×5 μm^2 rectangle to an 8×5 μm^2 obround-shaped channel increased the theoretical *Di* performance by approximately 590%, which suggests that the microbead-to-docking channel geometry match is a critical parameter for optimizing microfluidic bead-based diodes. For the current study, the fabrication process for generating a targeted circular-shaped channel was executed only once per docking channel (Fig. 3); however, prior studies have demonstrated that performing such procedures multiple times can improve the circularity of the microchannel[24], which provides an additional route for increasing the flow rectification potential of the microfluidic bead-based diode. The presented systems included overall microchannel heights of 18 μm, which, to the authors' knowledge, currently represent the thinnest microfluidic diodes demonstrated in the literature. Nonetheless, the systems included microbeads (15 μm in diameter) and microfeatures (*e.g.*, 15×15 μm^2 microposts) that were similar in size, which suggests that the current methodology could be scaled down further to achieve fluidic bead-based diodes at smaller size ranges as desired.

Experiments with multiple microfluidic bead-based diodes arrayed in parallel and in series revealed that such configurations can directly impact device functionality (Fig. 6; Fig. 7). These results could be attributed to the effects of microbead polydispersity on resistive capacity, as microbeads with non-ideal geometries could affect docking performance. Specifically, irregular microbead geometries could lead to: (*i*) improper docking, where fluid could readily bypass docked microbeads, resulting in undesired reverse flow, or (*ii*) improved docking, which would enable docked microbeads to more effectively obstruct reverse flow. For systems with multiple diodes arrayed in parallel, the adverse effects of poorly docked microbeads could dominate the effects of successfully docked beads. This would result in fluid being directed through channels with suboptimal docking, which offers a potential basis for the observed reduction in device performance associated with additional diodes in parallel. Conversely, in systems with multiple diodes arrayed in series, effectively docked microbeads could counteract the effects of deficient docking, which would support the trend of improved *Di* for higher numbers of diodes in series. These results suggest that increasing the number of microfluidic bead-based diodes in series could enable enhanced flow rectification; however, such modifications would also increase the pressure load required to achieve forward flow. These results may also provide insight into prior microfluidic bead-based diodes with larger numbers of microbeads. For example, prior reports observed that system configurations with thinner channels for reverse flow microbead docking outperformed systems with wider channels, despite the latter systems including larger numbers of beads and longer lengths (in certain cases)[22]. By approximating the wider channels as resembling systems with multiple microbeads in parallel, the results from the prior work would be consistent with the current study. Furthermore, the current results could inform the design of future versions of such multiple-bead diodes through two general approaches: (*i*) decreasing the width (while increasing the length) of the reverse flow microbead docking area, and (*ii*) increasing the width of the forward flow docking area. These predictions are consistent with the experimental observations reported in the prior work[22].

One challenge associated with microfluidic bead-based diodes is the loading of suspended microbeads into the diode chamber. Because the forms of manual placement typically employed for ball valves[18-20] are difficult to execute for singular, microscale particles, here we adapted the μPAR methodology[27] as a one-way track for pre-loading a single microbead into the system. This process is advantageous compared to prior methods because the number of microbeads loaded into the diode chamber can be well-regulated and issues stemming from particle size can be avoided. Consistent with the majority of microbead-loading procedures, however, manual observation and regulation are required. To limit or bypass these drawbacks, future works should investigate alternative methods for loading dynamic resistive elements

within diode chambers. For example, *in situ* fabrication techniques (*e.g.*, optofluidic lithography) and bottom-up construction processes (*e.g.*, micro/nanoscale 3D printing) could offer significant benefits for engineering such microfluidic components. Nonetheless, the experimental results for the presented microfluidic bead-based diode represent some of the largest *Di's* observed for low *Re* flow, and reveal important trends for device architectures with multiple diodes arrayed in parallel and in series. Thus, the current study provides a fundamental baseline for the design and implementation of future microfluidic diodes with dynamic resistive elements, which could greatly extend the efficacy of lab-on-a-chip systems in which flow rectification is critical, such as microscale drug delivery devices, micropumps, and integrated microfluidic circuits.

Acknowledgements

The authors greatly appreciate the help and support of Thomas Brubaker, Deepak Lingam, Casey Glick, Nazly Pirmoradi, William Krieger, Adrienne Higa, Roseanne Warren, Megan E. Dueck, and Paul Lum, as well as the members of the Liwei Lin Laboratory, the Biologically-inspired Photonics-Optofluidics-Electronics Technology and Science (BioPOETS) Laboratory, and the Micro Mechanical Methods for Biology (M^3B) Laboratory Program. This research was supported in part by the DARPA N/MEMS program under the Micro/Nano Fluidics Fundamentals Focus (MF3) center.

Notes and references

[a] Department of Mechanical Engineering

[b] Department of Bioengineering

Berkeley Sensor and Actuator Center

Biomolecular Nanotechnology Center

University of California, Berkeley

* 668 Sutardja Dai Hall, Berkeley, CA, 94720, USA, Tel: +1 410 935 8971; Fax: +1 510 643 6637; E-mail: rsochol@gmail.com

† Electronic Supplementary Information (ESI) available: SEM micrographs of fabrication results, sequential micrographs of the microbead pre-loading process, additional fabrication results, simulation meshes of various docking channel geometries, and additional simulation results; movies of the circular-shaped docking channel fabrication process, the microbead pre-loading process, and microbead dynamics during device operation. See DOI: 10.1039/b000000x/

1 A. Starr, *Nat Med*, 2007, **13**, 1160-1164.

2 K. W. Oh and C. H. Ahn, *Journal of Micromechanics and Microengineering*, 2006, **16**, R13-R39.

3 D. C. Leslie, C. J. Easley, E. Seker, J. M. Karlinsey, M. Utz, M. R. Begley and J. P. Landers, *Nature Physics*, 2009, **5**, 231-235.

4 B. Mosadegh, C.-H. Kuo, Y.-C. Tung, Y.-s. Torisawa, T. Bersano-Begey, H. Tavana and S. Takayama, *Nature Physics*, 2010, **6**, 433-437.

5 W. H. Tan and S. Takeuchi, *Proceedings of the National Academy of Sciences of the United States of America*, 2007, **104**, 1146-1151.

6 B. Mosadegh, T. Bersano-Begey, J. Y. Park, M. A. Burns and S. Takayama, *Lab on a Chip*, 2011, **11**, 2813-2818.

7 R. D. Sochol, B. P. Casavant, M. E. Dueck, L. P. Lee and L. Lin, *Journal of Micromechanics and Microengineering*, 2011, **21**, 054019.

8 J. A. Weaver, J. Melin, D. Stark, S. R. Quake and M. A. Horowitz, *Nature Physics*, 2010, **6**, 218-223.

9 B. Yang and Q. Lin, *Sensors and Actuators a-Physical*, 2007, **134**, 186-193.

10 J. Loverich, I. Kanno and H. Kotera, *Microfluidics and Nanofluidics*, 2007, **3**, 427-435.

11 K.-S. Yang, I.-Y. Chen, C.-C. Wang and J.-C. Shyu, *Microsystem Technologies-Micro-and Nanosystems-Information Storage and Processing Systems*, 2010, **16**, 1691-1697.

12 S. Lin, Y. Deng, Y. Wu and Z. Liu, Optimizing Tesla valve for inertial microfluidics, Dalian, China, 2012.

13 A. Groisman and S. R. Quake, *Physical Review Letters*, 2004, **92**.

14 M. L. Adams, M. L. Johnston, A. Scherer and S. R. Quake, *Journal of Micromechanics and Microengineering*, 2005, **15**, 1517-1521.

15 G. H. Feng and E. S. Kim, *Journal of Micromechanics and Microengineering*, 2004, **14**, 429-435.

16 W. Li, T. Chen, Z. Chen, P. Fei, Z. Yu, Y. Pang and Y. Huang, *Lab on a Chip*, 2012, **12**, 1587-1590.

17 J. J. Loverich, I. Kanno and H. Kotera, *Lab on a Chip*, 2006, **6**, 1147-1154.

18 T. R. Pan, S. J. McDonald, E. M. Kai and B. Ziaie, *Journal of Micromechanics and Microengineering*, 2005, **15**, 1021-1026.

19 A. Sin, C. F. Reardon and M. L. Shuler, *Biotechnology and Bioengineering*, 2004, **85**, 359-363.

20 C. Yamahata, F. Lacharme, Y. Burri and M. A. M. Gijs, *Sensors and Actuators B-Chemical*, 2005, **110**, 1-7.

21 M. C. Carrozza, N. Croce, B. Magnani and P. Dario, *Journal of Micromechanics and Microengineering*, 1995, **5**, 177-179.

22 K. Ou, J. Jackson, H. Burt and M. Chiao, *Lab on a Chip*, 2012.

23 R. D. Sochol, M. E. Dueck, S. Li, L. P. Lee and L. Lin, *Lab on a Chip*, 2012, **12**, 5051-5056.

24 R. D. Sochol, K. Iwai, J. Lei, D. Lingam, L. P. Lee and L. Lin, A Single-Microbead-Based Microfluidic Diode for Ultra-Low Reynolds Number Applications, *Proceedings of the IEEE 25th International Conference on Micro Electro Mechanical Systems (MEMS 2012)*, Paris, France, 2012.

25 R. D. Sochol, J. Lei, A. Lu, E. L. Hicks, S. Gao, V. Menon, L. P. Lee and L. Lin, Circular Microchannels Enhance Diodicity Performance at Ultra-Low Reynolds Number for Microfluidic Bead-Based Diodes, *Proceedings of the 16th International Conference on Miniaturized Systems for Chemistry and Life Sciences (μTAS 2012)*, Okinawa, Japan, 2012.

26 M. Abdelgawad, C. Wu, W.-Y. Chien, W. R. Geddie, M. A. S. Jewett and Y. Sun, *Lab on a Chip*, 2011, **11**, 545-551.

27 R. D. Sochol, S. Li, L. P. Lee and L. Lin, *Lab on a Chip*, 2012, **12**, 4168-4177.